Diagnostics of Nonradiative Defects in the Bulk and Surface of Brewster-Cut Ti:sapphire Laser Materials Using Photothermal Radiometry

Joseph Vanniasinkam, Mahendra Munidasa, Andreas Othonos, Milan Kokta, and Andreas Mandelis

***Abstract*— The understanding of the problem of nonradiative energy conversion in solid-state laser materials is a key factor in improving the overall efficiency of solid-state lasers. Furthermore, the reduction of the heat generated in an optically pumped laser crystal can lead to several new applications of solid-state lasers, especially in the high-power region. To improve the quality of grown crystals, laser crystal growers require accurate techniques to perform the quality control that is so vital to improving the growth process.**

Using a time-domain approach and a time-domain theoretical treatment of the IR radiative emission signal, it was determined that one may probe nonradiative surface and bulk processes by monitoring different time ranges. Our results show that photothermal radiometry can be used as a single-ended technique to evaluate both the bulk and surface nonradiative energy conversion rates in a solid-state laser material. This technique was compared to the standard laser cavity technique and it was concluded that photothermal radiometry can provide additional information to the standard technique by identifying the sources of heat generation as either surface- or bulk-originating.

***Index Terms*— Nondestructive evaluation, nonradiative energy conversion, photothermal radiometry, quality control, solid-state lasers.**

I. Introduction

SOLID-STATE lasers are currently finding wide application in research and industry due to their capabilities related to tunability and the ability to provide short pulses. A key factor that affects the performance of such a laser is the efficient conversion of the pump energy into useful laser output. This energy conversion is inhibited by nonradiative energy conversion processes, which can occur due to both intrinsic processes as well as the presence of growth defects [1]. The determination of the presence of heat-generating (nonradiative) defects in solid-state laser materials is of great interest to laser crystal growers who seek to adjust and improve the crystal growth process with a view toward a better quality yield.

Several groups have attempted to use a variety of techniques to characterize laser materials, including integrating spheres [2], photocaloric methods [3], [4], photoacoustic spectroscopy (PAS) [5]–[7], and photopyroelectric spectroscopy (PPES) [8], [9]. Upon evaluating these experimental techniques, we defined a set of criteria that are relevant to the problem of laser crystal evaluation in an industrial crystal growth setting. These criteria include the ability to:

1) perform the measurement in a noncontact, remote manner;
2) account for the presence of surface absorption, which has been shown to be an important factor that limits the overall efficiency of a laser crystal;
3) characterize both surface and bulk nonradiative energy conversion processes simultaneously, using a single technique.

Although PPES was used previously to determine both bulk and surface nonradiative energy conversion processes [8], this technique is not optimally suitable to meet the above criteria for two reasons. First, PPES is a technique where the front surface is irradiated and the back surface temperature is monitored. A more optimal approach would be to both irradiate and monitor the same surface. Second, the separation of bulk and surface absorption requires a pair of samples of different thickness with the same surface treatment. This restriction is not a very practical one under industrial conditions, due to the additional time and cost of cutting and polishing two sets of samples for one measurement. A more optimal technique was found in photothermal radiometry (PTR), which involves the detection of back-scattered infrared (IR) emission from a sample that is irradiated by an optical source [10]–[12]. Mandelis *et al.* [13], [14] were the first to apply PTR to the study of quantum efficiency and metastable lifetime in solid-state laser materials.

In this paper, we demonstrate that PTR can be used as an alternative to a standard method currently used for laser material diagnostics. The standard method of laser crystal quality evaluation is to determine the slope efficiency of a crystal aligned in a laser cavity [15], [16]. However, the slope efficiency cannot give a measure of the losses due to the laser material *only*. Since the slope efficiency is dependent on the cavity arrangement, this technique is limited in that one cannot compare two laser crystals of different growth conditions and/or sizes, which may be being used in two different cavities. Furthermore, the slope efficiency cannot give any insight into *why* a particular material is poorer than another

Manuscript received May 12, 1997; revised August 26, 1997.

J. Vanniasinkam, M. Munidasa, and A. Mandelis are with the Department of Mechanical and Industrial Engineering, Photothermal and Optoelectronic Diagnostics Laboratories, University of Toronto, Toronto, Ont., Canada, M5S 3G8.

A. Othonos is with the Department of Natural Sciences, University of Cyprus, Cyprus.

M. Kokta is with Union Carbide, Inc., Washougal, WA 98671 USA.

Publisher Item Identifier S 0018-9197(97)08404-2.

one. While these techniques may provide adequate information for some applications, they are unable to provide laser crystal growers with enough information about the grown crystals. A key requirement for the improvement in crystal growth processes and the growth of better quality laser materials is the development of a technique such as PTR so it can give the crystal grower useful information about both the sources of nonradiative energy conversion and their relative contributions to the overall losses in a crystal.

II. Theoretical Background

As discussed in more detail elsewhere [17], [18], the PTR technique has the ability to monitor nonradiative processes occurring in the bulk and surface simultaneously. By detecting the IR emission from a laser material at very short times after pulse cutoff, one can characterize the laser material surface. By detecting the IR emission at very long times after pulse cutoff, one obtains information about the bulk nonradiative energy conversion. Since this approach calls for time-domain detection, a theoretical model of the time-dependent IR emission from a crystal in response to a laser pulse was developed. The details of this treatment are given elsewhere [17], [18]. However, the final expressions for the early-time and late-time IR emission are shown below. These expressions are then used to curve-fit the experimental data obtained using PTR, following which the bulk and surface energy generation rates (as defined below) are obtained.

A. Early-Time Model

In the derivation of this model, a four-level laser system with the $2 \rightarrow 1$ level transition being the laser transition is assumed. τ denotes the lifetime of the upper laser level 2 whereas τ_{21} represents the lifetime of the laser transition. We can then write the equation governing early-time IR radiation emission from a laser crystal as [17]

$$S(t;\lambda_{\rm vis}) = \phi_1\tau(e^{\tau_{\rm p}/\tau_{21}} - e^{-W_{po}\tau_{\rm p}})e^{-t/\tau_{21}} + \phi_2\left[Y\left(\sqrt{\frac{t}{\tau_{\rm IR}}}\right) - Y\left(\sqrt{\frac{t-\tau_{\rm p}}{\tau_{\rm IR}}}\right) + \frac{2}{\sqrt{\pi\tau_{\rm IR}}}\left(\sqrt{t} - \sqrt{t-\tau_{\rm p}}\right)\right]. \quad (1)$$

The first term of the above equation represents the direct IR emission by stationary excited Ti^{3+} ions in the crystal. This term has a similar functional form as the luminescence transient. The second term represents the IR radiation emission due to nonradiative processes occurring at the surface. $\tau_{\rm IR}$ is a characteristic time based on the IR absorption coefficient of the sample and the thermal diffusivity α of the sample. $Y(x) \equiv \exp(x^2)\,\mathrm{erfc}\,(x)$, $W_{\rm po}$ is the pumping rate, and $\tau_{\rm p}$ is the input optical excitation pulse duration. The two fitting parameters are

$$\phi_1 = (1-\Gamma_{\rm s})B(T_\infty, \lambda_{\rm vis})W_{\rm po}N_{\rm T} \quad (2)$$

and

$$\phi_2 = \frac{2A(T_\infty, \lambda_{\rm vis})I_{\rm o}\Gamma_{\rm S}\alpha\tau_{\rm IR}}{\pi k}. \quad (3)$$

In the above equations, A and B are independent of time but depend on temperature and on the spectral range of the detector. $\Gamma_{\rm S}$ is the important surface absorptance parameter that we seek to find by fitting these equations to the experimental data, k is the thermal conductivity, and $\lambda_{\rm vis}$ is the wavelength of the excitation pulse. The curve-fitting process for the early time data results in the determination of the two fitting parameters ϕ_1 and ϕ_2 for a given crystal. In the expressions for ϕ_1 and ϕ_2, the only quantity that varies from crystal to crystal is the surface absorptance, $\Gamma_{\rm s}$. The other quantities such as k (thermal conductivity), α (thermal diffusivity), $W_{\rm po}$ (pumping rate), $N_{\rm T}$ (total population), $I_{\rm o}$ (optical intensity) can be assumed constant from sample to sample, given identical input pumping conditions. Also, A and B are constant from sample to sample, since these two parameters are multiplying constants that depend only on ambient temperature and the spectral range of the detector.

For a given crystal sample, the curve-fitting routine returns values of ϕ_1 and ϕ_2. For a given crystal sample i, we can rewrite (2) and (3) as $\phi_1^{(i)} = K_1(1-\Gamma_{\rm s}^i)$ and $\phi_2^{(i)} = K_2\Gamma_{\rm s}^i$, where K_1 and K_2 are the same for any crystal sample. If two crystals are evaluated, four equations with four unknowns [K_1, K_2, $\Gamma_{\rm s}$(Crystal 1), $\Gamma_{\rm s}$(Crystal 2)] can be written and then solved for the surface absorptance $\Gamma_{\rm s}$ of the two crystals. Finally, we define the surface nonradiative energy generation rate Q_s:

$$Q_{\rm s} = I_{\rm o}\Gamma_{\rm s}\ [\mathrm{W/m^2}]. \quad (4)$$

In what follows, the surfaces of different crystals will be characterized by the $Q_{\rm s}$ parameter, having first found $\Gamma_{\rm s}$ from the results of the curve fitting to experimental data.

B. Late-Time Model

In developing this model [18], it was assumed that the modulated IR radiation emission is proportional to the modulated temperature at the surface of the crystal $\theta(r, z, t)$ where r, z are the radial and depth coordinates and t represents time. The model predicts that at very long times after pulse cutoff the contribution of surface nonradiative processes to the temperature at the surface (denoted below by $\theta_{\rm s}$) is negligible compared to the contribution of bulk nonradiative processes. Thus, the equation governing late-time IR radiation emission from a laser crystal may be written as [18] as (5), shown at the bottom of the next page, where R is the laser beam spot-size and the function $f(t_o)$ is defined for times $t \geq \tau_{\rm p}$ as

$$(e^{\tau_{\rm p}/\tau_{21}} - e^{-W_{\rm po}\tau_{\rm p}})e^{-t_o/\tau_{21}} \cdot [1 - 2W_{\rm po}\tau(1-e^{-\tau_{\rm p}/\tau})e^{-(t_o-\tau_{\rm p})/\tau_{21}}]. \quad (6)$$

The fitting function ϕ_3 is given by

$$\phi_3 = \frac{2(1-\Gamma_{\rm s})\sqrt{\alpha}P_o\beta_{30}(E_{30}^{\rm NR}/E_{30})}{\pi k(1+W_{\rm po}\tau_{21})}. \quad (7)$$

The curve-fitting procedure for the late time data results in the determination of the fitting parameter ϕ_3 for a given crystal.

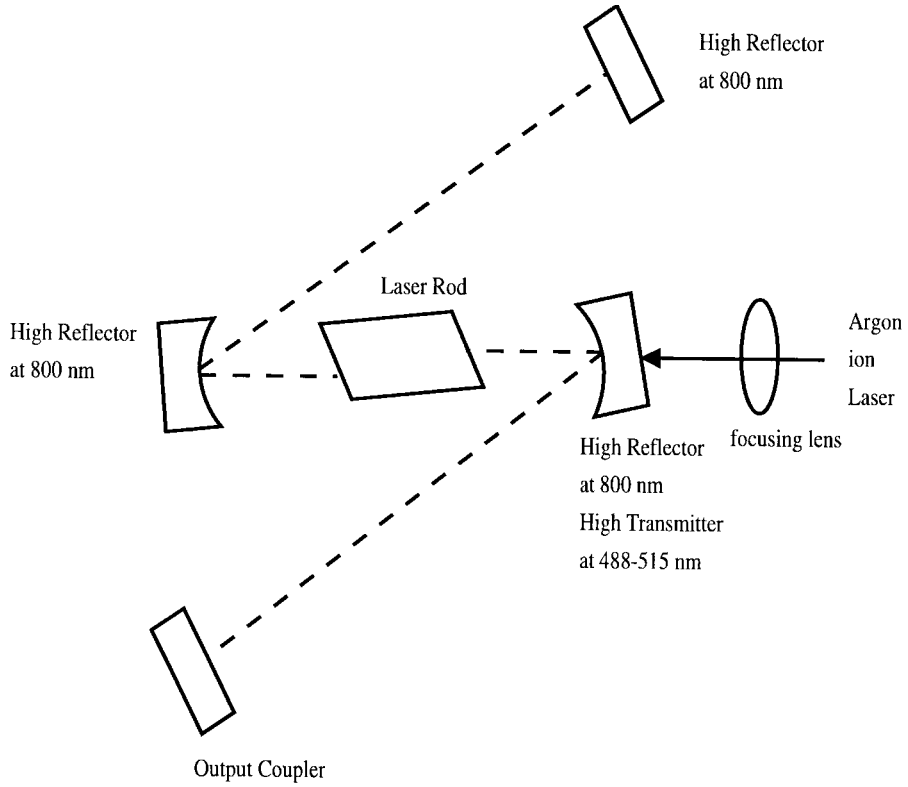

Fig. 1. CW Ti:sapphire four-mirror laser resonator.

In the expression for ϕ_3, the quantities α (thermal diffusivity), k (thermal conductivity), and $W_{\rm po}$ (pumping rate) are constant from crystal to crystal of the same material and have known numerical values [9]. The quantities that vary from crystal to crystal are the input power $P_{\rm o}$, the surface absorptance $\Gamma_{\rm s}$, the optical absorption coefficient at the pump wavelength β_{30}, the nonradiative energy released during a transition from the upper level to the ground state $E_{30}^{\rm NR}$, and the metastable state lifetime τ_{21}. The surface absorptance and the metastable state lifetime of a given crystal can be found by conducting early-time PTR experiments and luminescence measurements, respectively. τ_h and τ_β are characteristic thermal and photothermal transfer times, respectively, whose values for Ti : sapphire are known to be much larger than the time scales under which the experiment is performed [18]. Substituting the known values of $P_{\rm o}$, τ_{21}, $\Gamma_{\rm s}$, α, k, $W_{\rm po}$, and the fitting parameter ϕ_3 returned by the curve-fitting routine into (7), we obtain a numerical value for the parameter $\beta_{30}(E_{30}^{\rm NR}/E_{30})$. Finally, the bulk nonradiative energy generation rate $Q_{\rm b}$ is defined as

$$Q_{\rm b} = I_{\rm o}\beta_{30}(E_{30}^{\rm NR}/E_{30})\ [\text{W/m}^3]. \tag{8}$$

In this paper, the nonradiative bulk properties of different crystals were characterized by the $Q_{\rm b}$ parameter, by first finding $\beta_{30}(E_{30}^{\rm NR}/E_{30})$ from the results of the curve fitting to experimental data.

III. Experimental Approaches to Nonradiative Defect Characterization

A. Laser Cavity Method

A four-mirror folded cavity Ti:sapphire laser resonator was designed and built to evaluate the laser output performance of Ti:sapphire crystals. Fig. 1 shows the layout of this laser cavity. An argon ion laser operating multiline (488–514 nm) was used as the pump source. Longitudinal (end) pumping was used to produce a region of uniform gain in the crystal.

This method of pumping is very efficient for solid-state laser media because the pump beam and the lasing cavity mode are collinear over the entire length of the crystal [19]. Due to the low absorption of Ti:sapphire, it is necessary to provide a high pumping intensity into the Ti:sapphire medium. Such pumping

$$\theta(0,0,t) = \theta_{\rm s}(0,0,t) + \phi_3\left\{\int_0^t \frac{f(t_o)\ Y\left[\dfrac{\sqrt{(t-t_o)}}{\tau_h}\right]dt_o}{[1-\sqrt{\tau_h/\tau_\beta(t_o)}][8\alpha(t-t_o)+R^2]} - \sqrt{\tau_h}\int_0^t \frac{f(t_o)\ Y\left[\dfrac{\sqrt{(t-t_o)}}{\tau_\beta(t_o)}\right]dt_o}{[\sqrt{\tau_\beta(t_o)}-\sqrt{\tau_h}][8\alpha(t-t_o)+R^2]}\right\} \tag{5}$$

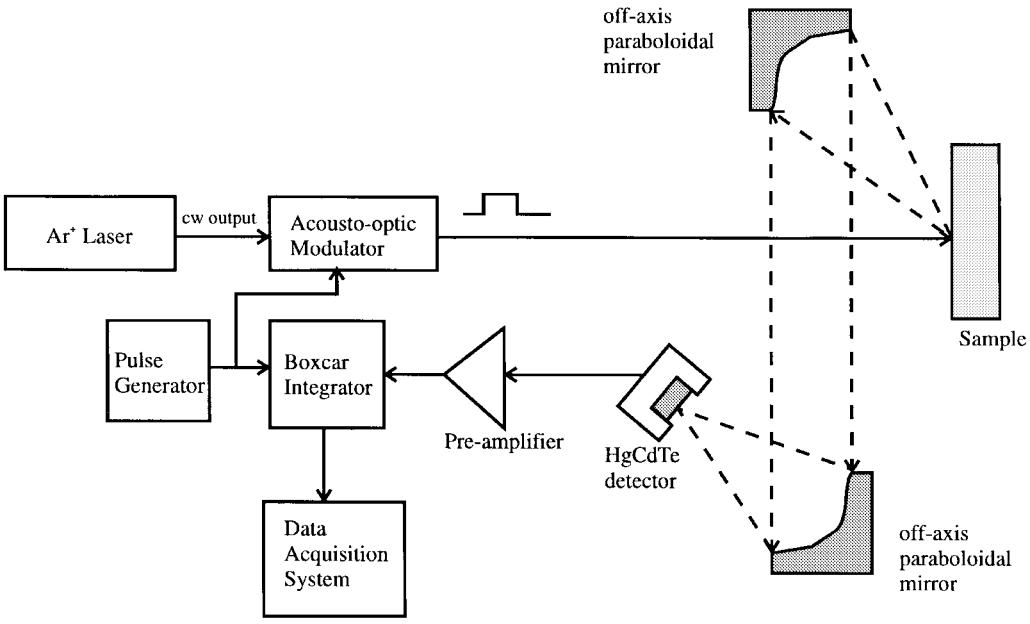

Fig. 2. Experimental layout of a photothermal radiometric detection system.

intensities can be achieved by tightly focusing the pump beam into the gain medium with the use of a pair of curved folding mirrors (radius of curvature = 10 cm). The Brewster-cut laser rod introduces a significant amount of astigmatic distortion to the beam, which can severely affect the beam quality of the laser. To compensate for this astigmatism, the two curved folding mirrors used to concentrate the beam into the laser gain medium are tilted off-axis by an appropriate amount [16]. The amount by which the mirrors are tilted depends on the length of the gain medium. The resonator is completed with a flat 10% transmission output coupler and high-reflecting flat mirror.

B. Photothermal Radiometry Method

The arrangement of the photothermal radiometry experiment is shown in Fig. 2. The CW output from an argon ion laser is modulated at the required pulse repetition rate and duty cycle by an acoustooptic modulator before impinging on the sample laser material. The sample is mounted on a sample holder that enables motion in three dimensions via translational stages. Absorption of the incident light and subsequent direct emission or nonradiative relaxation in the sample results in the sample emitting IR radiation. This radiation is collected and collimated by two off-axis paraboloidal mirrors, which then focus the radiation to an IR detector. The detector is a liquid-nitrogen-cooled photoconductive mercury–cadmium–telluride (MCT) detector, with a spectral bandwidth of 2–14 μm [20]. A Germanium window is installed on the face of the detector to prevent any visible light from entering the active area of the detector. The detector signal is then passed through a pre-amplifier with a 1-Hz low-frequency cutoff. This cutoff will reject any dc drift of the MCT detector signal and send the modulated ac signal to the boxcar integrator which reconstructs the transient signal.

The following approach was used to measure the transient IR emission profile of radiation emitted by the laser material in response to an optical excitation. The sample was irradiated by modulated Ar-ion laser light and allowed to reestablish thermal equilibrium with the surroundings. The drift in the IR emission signal (corresponding to the sample temperature) was monitored by a lock-in amplifier. After the lock-in signal became stable, the sample was aligned such that the beam waist was coincident with the front surface of the sample. This alignment is obtained by varying the position of the sample along the optical beam axis and monitoring the lock-in signal, which will yield a maximum value when the beam waist irradiates the front surface of the sample. With the sample in this position, the detector was aligned such that the energy collected by the parabolic mirrors has a focal point at the surface of the detector active area.

A repetitive pulse of a given duration and period irradiated the sample. With the pulse duration and period fixed, the boxcar integrator was used to reconstruct the transient profile of the IR emission from the sample in response to this pulse. In a typical reconstruction, the boxcar integrator would open a gate of a specified time at a specified location along the transient and average the measured signal over 10 000 cycles. The gate would then move to the next location along the transient and obtain an average over the next 10 000 cycles. When every point along a transient was averaged, the transient was reconstructed. To test whether instrumental effects were contributing to this transient emission, the transient instrumental response was also measured.

IV. Materials and Results

A. A Description of the Samples Tested

The primary difference between the laser crystal samples tested in the laser cavity and the samples evaluated using photothermal radiometry is their geometry. Those crystals were cylindrical rods with flat, polished end faces. In their

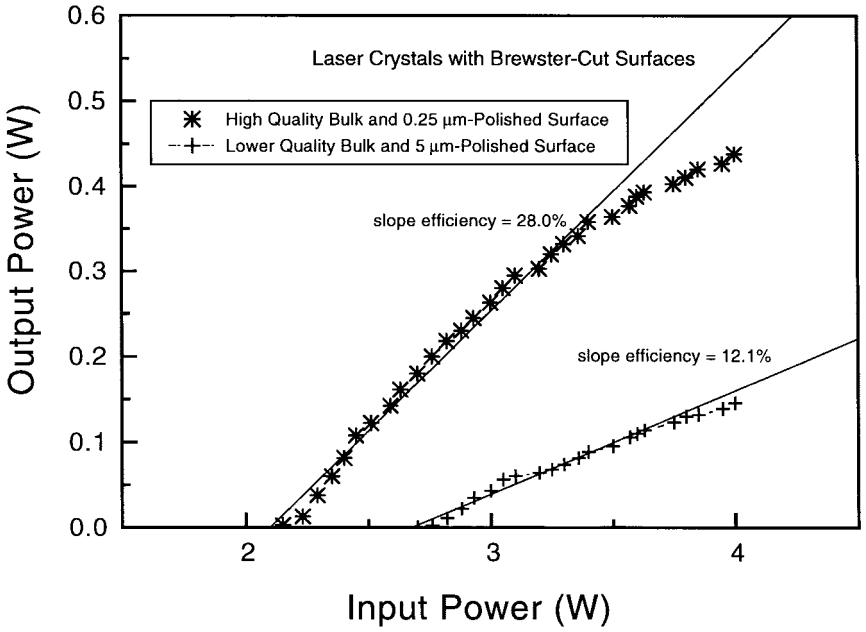

Fig. 3. Output power versus input power for two Brewster-cut laser rods, each having distinct surface and bulk properties.

present geometry, those crystals cannot be used to produce a working laser. The end faces of crystals used in lasers must be cut at Brewster's angle, since reflection losses can form a significant component of the total losses in a laser cavity.

Two Brewster-cut laser rods were evaluated in the cavity, each having different surface and bulk properties in relation to the other. One of the crystals had a high bulk figure-of-merit (FOM) and surfaces treated with the best available surface polish (polishing with 1-μm diamond particulates followed by polishing with 0.25-μm particulates). The other crystal had a lower bulk FOM and surfaces treated by polishing with 5-μm diamond particulates.

B. Laser Cavity Experiments to Determine Slope Efficiency

We evaluated the performance of the two Brewster-cut laser rods using the astigmatically compensated four-mirror laser resonator described above. For each crystal, the cavity was tuned to obtain lasing action after which the power of the 650–1100-nm Ti:sapphire laser output was measured as a function of 488–514 nm Ar-ion input pump power. Fig. 3 shows the input–output power curve for the two samples mentioned above. The figure shows that the slope efficiency of the crystal with the better quality bulk and the better quality surface is 28.0% and the laser crystal has a threshold lasing power of 2.1 W, whereas the lower quality crystal has a slope efficiency of 12.1% and a threshold lasing power of 2.7 W.

C. Radiometry Experiments to Determine Bulk and Surface Heating Losses

Following the laser cavity experiments which were used to measure the optical output of the crystals, photothermal radiometry was utilized to measure the thermal energy generated in the same two crystals, which contributes to the losses in the laser. For each crystal, both early-time and late-time radiometry experiments were conducted to characterize their surface and bulk properties. The transient early-time IR radiation emission is shown in Fig. 4, monitored in the 50–100-μs time range after the pulse is cut off. The figure shows that the 5-μm polished surface exhibits a faster decay than the 0.25-μm polished surface. Upon fitting these data to the early-time theoretical model given by (1), the value of the surface nonradiative energy generation rate $Q_{\rm s}$ was obtained from the fitting parameters described earlier. For the high bulk FOM crystal with the 0.25-μm polished surface, we obtained a $Q_{\rm s}$ value of 0.175 $I_{\rm o}$ [W/cm^2], and the low bulk FOM crystal with the 5-μm polished surface had a $Q_{\rm s}$ of 0.221 $I_{\rm o}$ [W/cm^2]. These quantities have been expressed as a function of the input optical intensity $I_{\rm o}$ [W/cm^2].

To evaluate and compare the bulk heating properties of the two crystals, we conducted late-time measurements in the 0–10-ms range after pulse cutoff. Fig. 5 shows the late-time IR radiation emission profiles for the two samples; a faster decay for the lower quality bulk was observed.

Upon fitting these curves to the theoretical late-time expressions for the transient temperature evolution in the crystal given by (5), we obtain from the fitting parameters a value for the bulk nonradiative energy generation rate $Q_{\rm b}$. For the high bulk FOM crystal with the 0.25-μm polished surface, the $Q_{\rm b}$ value of 0.11 $I_{\rm o}$ [W/cm^3] was calculated and the low bulk FOM crystal with the 5-μm polished surface had a $Q_{\rm b}$ of 0.17 $I_{\rm o}$ [W/cm^3]. These quantities have also been expressed as a function of the input optical intensity $I_{\rm o}$ [W/cm^2].

D. Monitoring Surface Polish Improvements

Upon completing the entire set of measurements described in the two previous sections, the surface quality of the lower

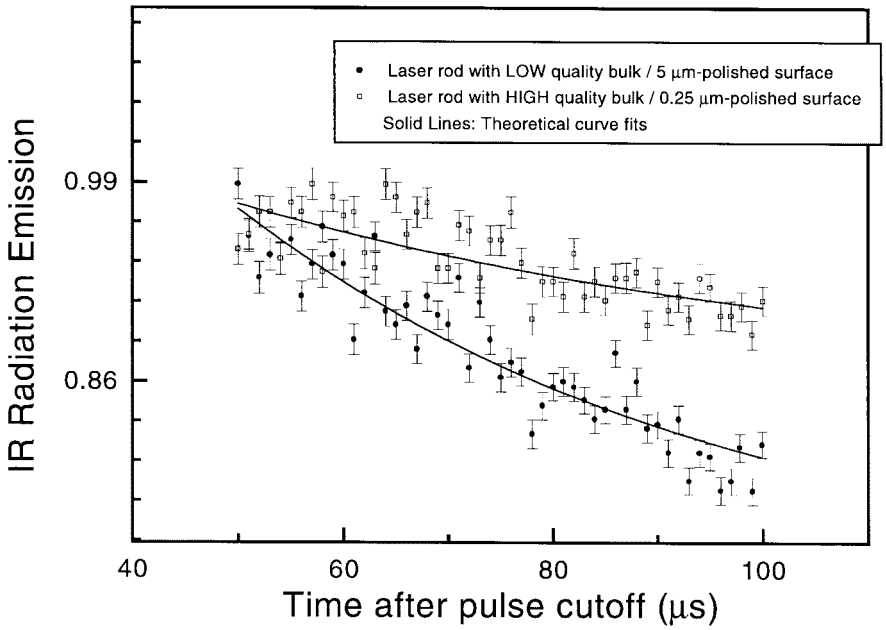

Fig. 4. IR radiation emission (normalized by its value at pulse cutoff) from a high bulk and surface quality laser rod and a low bulk and surface quality laser rod, measured in the early-time μs range where bulk effects are not felt and surface effects dominate. For a description of how each point on the graph is obtained, refer to the Appendix.

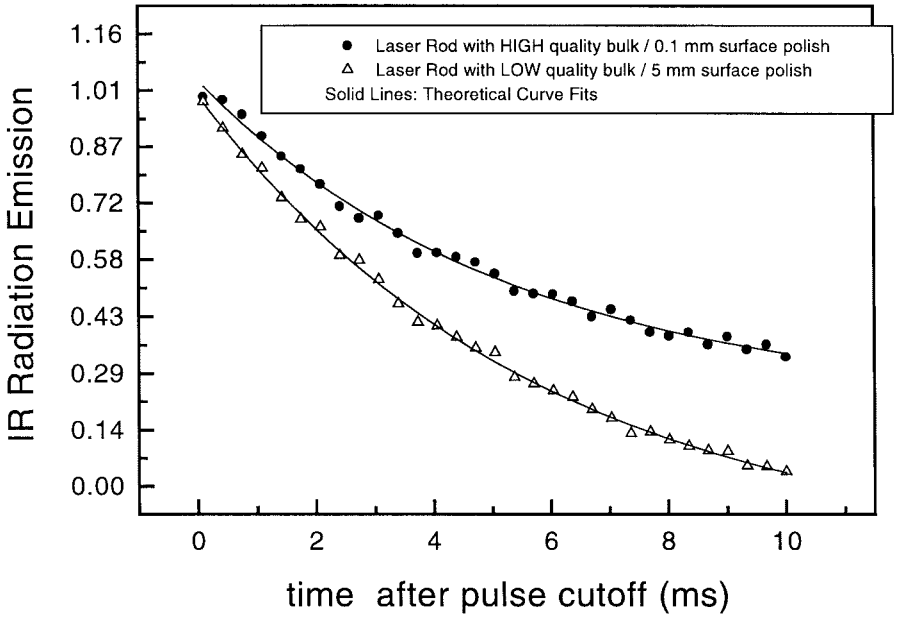

Fig. 5. IR radiation emission (normalized by its value at pulse cutoff) from a high bulk and surface quality laser rod and a low bulk and surface quality laser rod, measured in the late-time μs range where surface effects are not felt and bulk effects dominate. For a description of how each point on the graph is obtained, refer to the Appendix.

quality crystal was improved by polishing the crystal with the highest available grade of polish (polishing with 1-μm diamond particulates followed by polishing with 0.25-μm particulates). The laser cavity experiments were then repeated, as well as the radiometry experiments with the new sample to study the effect of surface improvement in laser materials.

Fig. 6 shows the output power as a function of input power for the crystal with the improved surface in comparison with itself before surface improvement and in comparison with the high-quality crystal. Note that the improvement of the surface has improved the slope efficiency of the laser, but not to the extent that the crystal is as good as the high bulk FOM crystal with the 28% slope efficiency. This was so because the crystal with the 28% slope efficiency had a better quality bulk *and* surface than the other crystal. Improvements in surface quality of the poorer crystal result in an improvement in slope efficiency to 17.5% from 12.1%. After this surface improvement, the differences between the crystal with 28%

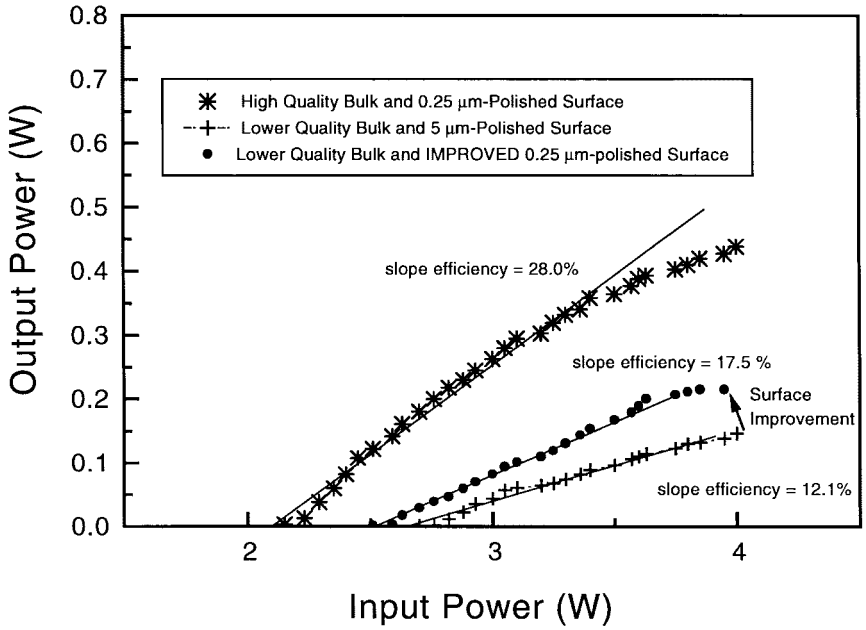

Fig. 6. Output power versus input power for two Brewster-cut laser rods. Data for the lower quality rod is shown before and after surface treatment. IR radiation emission (normalized by its value at pulse cutoff) from a low bulk quality laser rod before and after surface treatment, measured in the early-time μs range where bulk effects are not felt and surface effects dominate. For a description of how each point on the graph is obtained, refer to the Appendix.

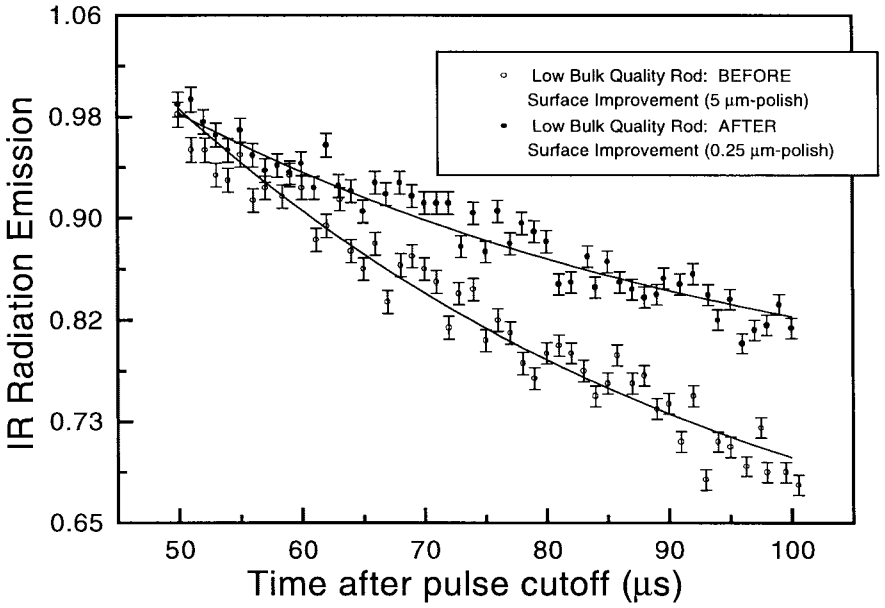

Fig. 7. IR radiation emission (normalized by its value at pulse cutoff) from a low-bulk-quality laser rod before and after surface treatment, measured in the early-time microsecond range where bulk effects are not felt and surface effects dominate. For a description of how each point on the graph is obtained, refer to the Appendix.

slope efficiency and the surface-improved crystal with 17.5% slope efficiency are due primarily to the differences in bulk quality.

We also conducted photothermal radiometry experiments of the crystal before and after surface polish improvements and compared these results with the laser cavity output data. Fig. 7 shows the radiometric emission profiles for the low bulk FOM crystal before and after surface modification in the 50–100-μs time range after the pulse is cut off. Upon curve fitting these results to (1), it was found that the surface energy generation rate $Q_{\rm s}$ improved from $Q_{\rm s} = 0.22I_{\rm o}$ before surface treatment to $Q_{\rm s} = 0.18I_{\rm o}$ after surface treatment. This new value of $Q_{\rm s}$ is very close to the value of $Q_{\rm s} = 0.175I_{\rm o}$ for the crystal that was originally polished with the highest quality process. Fig. 8 shows the radiometric emission profiles for the low bulk FOM crystal before and after surface modification in the 0–10-ms range. Since the bulk properties of the crystal do not change during the surface processing, the bulk properties are expected to remain unchanged. By curve fitting to obtain the bulk energy generation rate $Q_{\rm b}$, it was found that the $Q_{\rm b}$ value after surface treatment was almost the same as the value before the surface was modified.

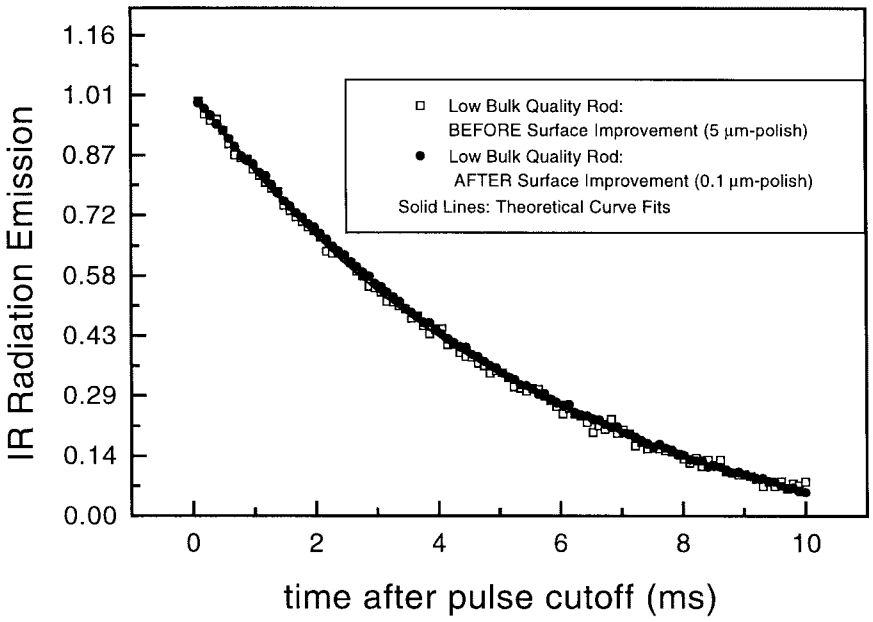

Fig. 8. IR radiation emission from a low-bulk-quality laser rod before and after surface treatment, measured in the late-time microsecond range where surface effects are not felt and bulk effects dominate. For a description of how each point on the graph is obtained, refer to the Appendix.

V. Discussion

The input–output power characteristics of the two laser crystals shown in Fig. 3 exhibit straight line behavior except at higher powers, where the output power stops increasing linearly with input power. This deviation from linearity is due to the temperature dependence of the radiative and nonradiative lifetimes. At higher powers, the temperature of the crystal increases, promoting more nonradiative activity. As a result, the laser output power increases sublinearly with respect to the input power.

Based on the experimental results described in the previous section, the standard method of laser material characterization (i.e., the slope efficiency from laser cavity output measurements) with our alternative method of characterization via photothermal radiometry can be compared. There are three main reasons for which PTR is a more suitable method of characterization.

1) In the standard method, the measured parameter is the slope efficiency, which is an "overall" efficiency parameter affected by the pumping efficiency, the output coupling efficiency, the mode cross-section efficiency, and the material quantum efficiency. By comparison, PTR gives a measure of the net nonradiative energy generated in the crystal, which is a more direct measure of the optical quality of the *material* as opposed to the overall efficiency of a laser resonator.
2) Given two crystals A and B, both the laser cavity output method and the PTR method can tell if A is "better" than B or vice versa. However, the laser cavity method cannot tell *why* crystal A is better than crystal B. In particular, the laser cavity method cannot tell if crystal A is better than B because it has a better quality surface, a better quality bulk, or both. Conversely, PTR can evaluate the bulk and surface quality independently of each other from a single sample, and with a single experimental setup.
3) From the standpoint of laser material quality control, PTR is a much more practical technique to use than the laser cavity approach. Having implemented both experimental systems in our laboratory, we observed the fact that the laser cavity is far more difficult to align and also far more sensitive to misalignment. It was noted that there are about 10 different alignment knobs in the laser cavity to which the laser output is very sensitive. By comparison, the PTR technique is only highly sensitive to one such alignment. Another practical issue relates to sample size. Using the laser cavity method, it is not very accurate to compare two samples of different sizes because the cavity parameters usually change. Conversely, the radiometry technique can be applied to samples of different sizes and to their bulk and surface quality, independently of their size.

Although the PTR technique has been demonstrated here for Ti:sapphire samples, it can be applied to a wide variety of solid-state laser materials given that three parameters can be measured: the absorption spectra, the fluorescence emission spectra, and the fluorescence lifetime. For a given laser material, it is important to know the absorption spectrum in the range of wavelengths associated with the optical pumping of the material. This data will allow the experimenter to select a pump laser wavelength appropriate for exciting the metastable state of the laser crystal in a PTR experiment. The fluorescence emission range is also a key issue in such an experiment. If the fluorescence emission spectrum overlaps the spectral range of the IR detector, the measured signal will then be due to a combination of radiative emission and lattice-temperature-related thermal (IR) emission, thus

complicating the analysis of the data obtained. This problem is most likely for materials exhibiting fluorescence in the near infrared range. It is advisable to work with a detector that has a low-wavelength cutoff of about 10 μm. The fluorescence lifetime of the material is an important parameter since it allows the determination of the lifetime of the laser transition, assuming that the quantum efficiency is also known. However, in terms of the PTR technique, it is the magnitude of the nonradiative lifetime that affects the timescales over which the measurements are performed. If the nonradiative processes are very fast compared to the detection timescales, the time it takes for the thermal energy released within the crystal to diffuse to the surface becomes the primary determining factor of the timescale involved in PTR detection.

Two further issues will affect how the PTR experiments are performed on a particular laser material. One is whether or not the material is inhomogeneously broadened. If the active ions in the material are distributed among sites which are subjected to varying degrees of pertubation from the surrounding crystal, the quantum efficiency of the ion will be dependent on the particular site it occupies. If a narrow-band laser is used in the PTR experiment on an inhomogeneously broadened material, some sites will be preferentially excited over others. In such cases, different excitation wavelengths will give rise to different combinations of excited sites and consequently to different measured values of η_{NR}. Another effect to consider is excited state re-absorption from the upper laser level to higher states. Although not present in Ti:sapphire, these effects are present in materials such as heavily doped ruby. Such effects limit the useful power emitted by the laser. To avoid having to include such effects in this analysis, it is important to ensure that optical intensities used in the photothermal experiments do not approach the nonlinear limit. This effect has been shown to be nonlinear in the incident light intensity, since it depends on the population of the upper laser level. One way of ensuring that such effects are not significant is to vary the input power and see if the resulting photothermal signal is linear with input power.

VI. Conclusion

It has been shown that the PTR technique has the capability of yielding the bulk nonradiative energy generation rate and the surface nonradiative energy generation rate with a single experimental configuration. Because of its remote, noncontact nature, the PTR technique is also capable of monitoring the quality of a laser crystal *in situ*, under the exact conditions in which the laser material is intended to operate. The pump source used in the PTR experiment can be the very source which pumps the material when it operates as a solid-state laser.

It has also been shown that the standard laser cavity method of laser crystal quality evaluation cannot give a measure of the losses due to the laser material *only*. Since the slope efficiency is dependent on the cavity arrangement, this technique is limited in that one cannot compare two laser crystals of different sizes. Furthermore, this technique cannot give insights into the relative contributions of the surface and the bulk. PTR can give the crystal grower useful information about both the sources of nonradiative energy conversion and their relative contributions to the overall losses in a crystal.

Appendix
PTR Data Acquisition

In the photothermal radiometric experiments, each data point on a given transient IR emission profile was obtained as follows. At a given time after pulse cutoff, each point on the graph represents the average value of the signal measured by the open gate over 10 000 cycles. The data acquisition program was written in such a manner that after a specified number of samples were obtained at one particular location in time, the averaging process would be repeated if the signal-to-noise ratio (SNR) did not exceed a specified amount. In this case, the SNR we specified was 100. Therefore each point on the transient profile has been obtained with a SNR of at least 100.

References

[1] W. Koechner, *Solid State Laser Engineering*, 3rd ed. New York: Springer-Verlag, 1992.

[2] C. E. Byvik and A. Buoncristiani, "Analysis of vibronic transitions in titanium doped sapphire using the temperature of the flourescence spectra," *IEEE J. Quantum Electron.*, vol. QE-21, pp. 1619–1623, 1985.

[3] A. J. Ramponi and J. A. Caird, "Fluorescence quantum efficiency and optical heating efficiency in laser crystals and glasses by laser calorimetry," *J. Appl. Phys.*, vol. 63, no. 11, pp. 5476–5484, 1988.

[4] Y. Li, I. Duncan, and T. Morrow, "Absolute fluorescence quantum efficiency of titanium-doped sapphire at ambient temperature," *J. Lumin.*, vol. 52, pp. 275–276, 1992.

[5] R. S. Quimby and W. M. Yen, "Photoacoustics measurement of absolute quantum efficiencies in solids," *Opt. Lett.*, vol. 3, no. 5, pp. 181–183, 1978.

[6] ———, "Photoacoustic measurement of the ruby quantum efficiency," *J. Appl. Phys.*, vol. 51, no. 3, pp. 1780–1782, 1980.

[7] M. L. Shand, "Quantum efficiency of alexandrite," *J. Appl. Phys.*, vol. 54, no. 5, pp. 2602–2604, 1983.

[8] J. Vanniasinkam, A. Mandelis, S. Buddhudu, and M. Kokta, "Photopyroelectric deconvolution of bulk and surface optical absorption and nonradiative energy conversion efficiency spectra in Ti:sapphire crystals," *J. Appl. Phys.*, vol. 75, pp. 8090–8097, 1994.

[9] A. Mandelis, J. Vanniasinkam, S. Buddhudu, A. Othonos, and M. Kokta, "Absolute nonradiative energy-conversion-efficiency spectra in Ti:sapphire crystals measured by noncontact quadrature photopyroelectric spectroscopy," *Phys. Rev. B*, vol. 48, pp. 6808–6821, 1993.

[10] R. D. Tom, E. P. O'Hara, and D. Benin, "A generalized model of photothermal radiometry," *J. Appl. Phys.*, vol. 53, no. 8, pp. 5392–5400, 1982.

[11] R. Santos and L. C. M. Miranda, "Theory of the photothermal radiometry with solids," *J. Appl. Phys.*, vol. 52, no. 6, pp. 4194–4198, 1981.

[12] P. E. Nordal and S. O. Kanstad, "New developments in photothermal radiometry," *Infrared Phys.*, vol. 25, no. 1, pp. 295–304, 1985.

[13] A. Mandelis, M. Munidasa, and A. Othonos, "Single-ended photothermal radiometric measurement of quantum efficiency and metastable lifetime in solid-state laser materials: The case of ruby," *IEEE J. Quantum Electron.*, vol. 29, pp. 1498–1504, 1993.

[14] A. Mandelis, Z. H. Chen, and R. Bleiss, "Quantum efficiency and metastable lifetime measurements in solid-state laser materials via lock-in rate-window photothermal radiometry: Technique and application to ruby ($Cr:Al_2O_3$)," *Opt. Eng.*, vol. 32, pp. 2046–2053, 1993.

[15] O. Svelto, *Principles of Lasers.* New York: Plenum, 1989.

[16] J. F. Pinto, L. Esterowitz, G. H. Rosenblatt, M. Kokta, and D. Peressini, "Improved Ti:sapphire laser performance with new high figure of merit crystals," *IEEE J. Quantum Electron.*, vol. 30, pp. 2612–2616, 1994.

[17] J. Vanniasinkam, A. Mandelis, M. Munidasa, and M. Kokta, "Deconvolution of surface and direct metastable-state blackbody emission in Ti:sapphire laser materials using boxcar time-domain photothermal radiometry," *J. Opt. Soc. Amer.*, to be published.

[18] A. Mandelis and J. Vanniasinkam, "Theory of nonradiative decay dynamics in solid-state laser media via laser photothermal diagnostics," *J. Appl. Phys.*, vol. 80, pp. 6107–6119, 1996.
[19] A. J. Alfrey, "Modeling of longitudinally pumped CW Ti:sapphire laser oscillators," *IEEE J. Quantum Electron.*, vol. 25, pp. 760–766, 1989.
[20] *Infrared Detectors 1994*, Judson EG and G Optoelectronics, 1994.

Joseph Vanniasinkam received the B.S. degree in mechanical engineering from the University of Texas at Austin in 1991 and the M.Eng. and Ph.D. degrees in mechanical engineering from the University of Toronto, Toronto, Ont., Canada, in 1993 and 1997, respectively. His doctoral research involved the use of optical methods to monitor nonradiative relaxation processes in solid-state laser materials.

After completing his undergraduate degree, he interned at NASA Johnson Space Center, Houston, TX. He is currently an Optical Engineer with Ultratech Stepper, San Jose, CA, working in the area of semiconductor microlithography.

Mahendra Munidasa received the B.Sc. degree in physics from the University of Colombo, Sri Lanka, in 1980 and the M.A. degree in physics and the Ph.D. degree in applied physics from Wayne State University, Detroit, MI, in 1983 and 1988, respectively.

Since 1989, he has been a Research Associate with the Photothermal and Optoelectronic Diagnostics Laboratories, Department of Mechanical Engineering at the University of Toronto, Ont., Canada. His current research interests are in method development and instrumentation for thermal-wave NDE.

Dr. Munidasa is a member of the American Physical Society.

Andreas Othonos received the B.Sc., M.Sc., and Ph.D. degrees in physics from the University of Toronto, Toronto, Ont., Canada, in 1984, 1986, and 1990, respectively. His doctoral dissertation research was conducted in the area of carrier and phonon dynamics in semiconductors.

From 1990 to 1995, he was a Research Scientist with the Ontario Laser and Lightwave Research Center. He is currently with the Department of Natural Sciences, University of Cyprus, Cyprus. He has published more than 35 papers in various refereed journals, along with a number of invited chapters in books and invited review papers. His current research interests are ultrafast carrier dynamics in semiconductors, nonlinear optics, fiber optic lasers, and fiber Bragg gratings.

Milan Kokta received the D.E.Sc. degree from Newark College of Engineering, Newark, NJ, in 1972.

From 1972 to 1974, he conducted post-doctoral research at Bell Laboratories, Murray Hill, NJ. He was with Allied Chemical Corporation, Morristown, NJ, from 1974 to 1977. Since 1977, he has been with Union Carbide Crystal Products, Washougal, WA, where he currently is Senior Staff Scientist and Research and Development Manager. He has been involved in crystal chemistry in the growth of oxide crystals for the past 25 years.

Andreas Mandelis received the B.S. degree in physics from Yale University, New Haven, CT, and the M.A. degree in applied physics, the M.S.E. degree in mechanical and aerospace engineering, and the Ph.D. degree in applied physics from Princeton University, Princeton, NJ.

From 1979 to 1981, he was a Member of the Scientific Staff with Bell-Northern Research, Ottawa, Canada, involved in silicon research and development. Since 1981, he has been with the University of Toronto, Toronto, Ont., Canada, where he is currently a Professor of Mechanical, Industrial, and Electrical Engineering and directs the Photothermal and Optoelectronic Diagnostics Laboratory. He has published more than 150 research papers in refereed journals, co-authored two books, including *Physics, Chemistry and Technology of Solid-State Gas Sensor Devices*, holds two patents, and has been Editor-in-Chief of the series "Progress in Photothermal and Photoacoustic Science and Technology." His research interests are photothermal instrumentation and measurement science and applications to electronic and manufacturing materials nondestructive evaluation.

Dr. Mandelis is a fellow of the American Physical Society.